Modeling of Battery Degradation in Electrified Vehicles

Olof Juhlin

LIU LINKÖPING UNIVERSITY

Master of Science Thesis in Electrical Engineering

Modeling of Battery Degradation in Electrified Vehicles

Olof Juhlin

LiTH-ISY-EX–16/5015–SE

Supervisor: **Christofer Sundström**
ISY, Linköpings universitet

Examiner: **Mattias Krysander**
ISY, Linköpings universitet

Division of Vehicular Systems
Department of Electrical Engineering
Linköping University
SE-581 83 Linköping, Sweden

Abstract

This thesis provides an insight into battery modeling in electric vehicles which includes degradation mechanisms as in automotive operation in electric vehicles. As electric vehicles with lithium ion batteries increase in popularity there is an increased need to study and model the capacity losses in such batteries. If there is a good understanding of the phenomena involved and an ability to predict these losses there is also a foundation to take measures to minimize these losses.

In this thesis a battery model for lithium ion batteries which includes heat dissipation is used as groundwork. This model is expanded with the addition of capacity losses due to usage as well as storage. By combining this with a simple vehicle model one can use these models to achieve an understanding as to how a battery or pack of several batteries would behave in a specific driving scenario. Much of the focus in the thesis is put into comparing the different factors of degradation to highlight what the major contributors are.

The conclusion is drawn that heat is the main cause for degradation for batteries in electric vehicles. This applies for driving usage as well as during storage. As heat is generated when a battery is used, the level of current is also a factor, as well as in which state of charge region the battery is used.

Acknowledgments

It has been very rewarding to work in a field which is so very relevant in this day. I would like to thank my examiner Mattias Kryssander and supervisor Christofer Sundström of Linköping University for giving me the opportuniy to do this thesis and also providing guidance and helpful discussions along the way.

I also thank the other students doing their thesis work at vehicular systems simultaneous to me and with whom I shared office. It was always a friendly environment and I believe that we all benefited from the discussions and help we could give each other.

Contents

1

Introduction

In this introducing chapter the general purpose of the thesis is presented. Some background on batteries in vehicles and also some basics regarding batteries and battery modeling which is needed to understand the following chapters of the thesis are given.

1.1 Background

In recent years electric vehicles (EV) have gained popularity and many car manufacturers are developing such vehicles in order to be a part of this emerging market. Electric vehicles are in this thesis divided into battery electric vehicles (BEV), hybrid electric vehicles (HEV) and plug-in hybrid electric vehicles (PHEV). A BEV draws all its power from the battery while hybrid variants also feature an internal combustion engine (ICE).

An essential part of these vehicles is the battery. The battery in a BEV is somewhat analogous to the fuel tank in a regular car with only an ICE, and as such is the limiting factor as to how far the vehicle may travel without charging. In an HEV or PHEV battery limitation can be described as to which extent you may depend on all electric drive.

There are many aspects to take into consideration regarding batteries when designing an EV. Batteries are expensive and large in volume and therefore it is desirable to use them as effectively as possible. There is also degradation in batteries, i.e. they will loose capacity and eventually be drained to the point where they are no longer functional. The main focus of this thesis is to model this degradation and to understand mechanisms affecting the state of health (SoH) of the battery. In order to prolong lifetime of the batteries in electric vehicles car manufacturers want to have an as low degradation rate as possible in their batteries.

The batteries used in these vehicles are packs of batteries consisting of individual cells connected in some configuration of series and parallel circuits. Degradation of the battery pack will be depending on the degradation of the individual cells as well as specific properties of the pack such as thermal characteristics, which will vary on how the cells are organised with respect to each other and the thermal management system. The specific chemistries of the cell as well as the packaging style of the cell, e.g. cylindrical or prismatic, is also of importance.

Battery modelling is used for gathering information on how the cells and battery packs will behave without testing on actual batteries, though the models need to be accurate to provide dependable simulations.

1.2   Objective

The main purpose of the thesis is to investigate what factors influence lithium-ion battery degradation and to which extent. This should be used to be able to make assessments on how a battery cell would degrade in specific situations. The method for investigating this is to develop a model for evaluating degradation in batteries. Using specified data in terms of cell configuration, temperature and charging/discharging usage, one should be able to get a state of health estimation of a battery cell or pack.

By connecting cells together and accounting for heat exchange between cells, simulations should be possible for packs of cells as found in electric vehicles and also be able to asses the level of degradation for a pack of a specified configuration during certain operating conditions.

1.2.1   Method

To model battery behaviour some basic knowledge on batteries is needed. The material in [11] provides basic as well as in depth knowledge about batteries in general and also devotes a chapter to lithium ion chemistries (Li-Ion), which is the chemistry that will be considered in this thesis. The work in [1] focuses on battery management systems (BMS) and gives an insight in how battery cells behave in packs and how to control them. Information on the propulsion of the EV, in which the battery is a significant part, can also be found in [5].

The models used in this thesis are of electrical circuit type and model the battery cell as a circuit of resistances and capacitors. In Figure 1.1 a model consisting of a voltage source and a resistance in series with a parallel branch of a resistance and a capacitor (RC-branch) is shown. Typically the electrical model is extended with more RC-branches to capture dynamics better. This comes with the price of greater model complexity.
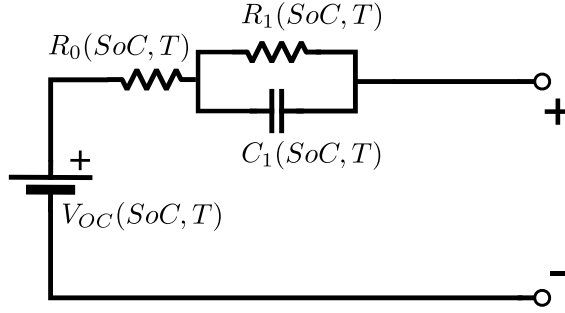
Figure 1.1: *Electrical model of a battery using one RC-branch*

In addition to degrading over time, a battery cell which has not been subject to degradation would not have identical performance during every cycle. As presented in the model in Figure 1.1, the properties of the components will vary depending on the state of charge (SoC) and temperature. A method for taking this into consideration is to use look-up tables in MATLAB, provided in [6], along with a thermal model for cell heat dissipation. Battery cell data as well as Simulink and Simscape models are provided along with [6] which are easily set up to create a battery pack that can be charged and discharged using a preconfigured current signal. These models will make up a foundation to be expanded upon in this thesis work.

This model uses power dissipation due to ohmic heating along with a heat equation for a homogeneous body,

$$C_T \frac{dT}{dt} = -\frac{T - T_a}{R_T} + P_S \tag{1.1}$$

where P_S is the power generated inside the cell, R_T the thermal resistance of the cell, T_a the ambient temperature and C_T the heat capacitance. By applying a laplace transformation, the average temperature inside a cell, $T(s)$ is computed as

$$T(s) = \frac{P_s R_T + T_a}{1 + R_T C_T s}. \tag{1.2}$$

The authors of [6] along with others also proposed a model consisting of three RC-branches to capture the dynamics of a lithium iron phosphate battery in [7]. An extra RC-branch utilizing a large time constant can be used if one wants to capture the hysteresis behaviour that exists when comparing charging to discharging, i.e. the relationship between SoC and open circuit voltage will differ when comparing charging to discharging. This is also covered in [2] which proposes a slightly different model, using a resistance dependent on whether the battery is charging or discharging to model this hysteresis.

In [3] an equivalent circuit model with two RC-branches is used to suggest a general purpose battery modelling approach.

Figure 1.2 depicts model accuracy depending on the number of RC-branches for a battery cell as presented in [7]. The figure shows a voltage rise that occurs

after a discharge pulse. The equivalent circuit model is discussed in more detail in the next section.
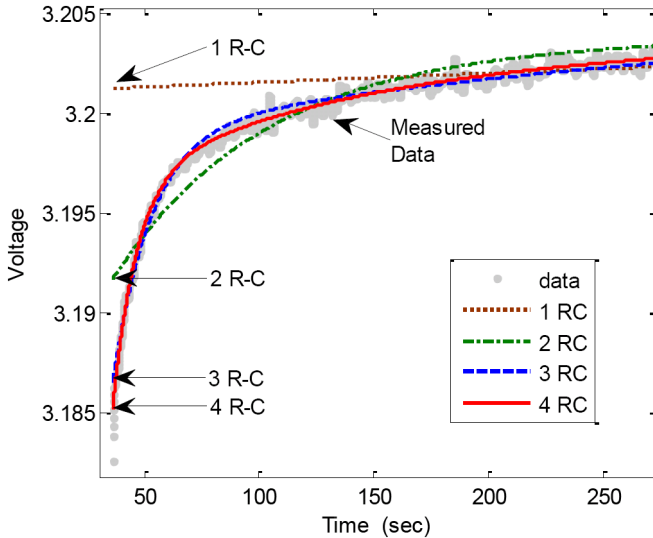
Figure 1.2: Close level model validation of battery cell models [7]

A physical interpretation of the equivalent circuit model using one and two RC-branches can be found in [11]. The lone resistance is the electrolyte solution resistance. In the RC-branch the resistance is the charge transfer resistance and the capacitance is the double layer capacitance. Extending with a second RC-branch can be seen as the capacity and impedance of a solid electrolyte interface (SEI) film that forms when the anode and electrolyte reacts in a Li-Ion cell.

In this thesis electrical circuit models will be used to model battery behaviour. One RC-branch is found to be sufficient as the close level accuracy given by an increased number of branches does not have a significant effect on degradation modeling. The electrical circuit model is then extended to incorporate battery degradation to estimate the batteries state of health. This is discussed in section 1.2.3.

1.2.2   Equivalent circuit model evaluation

The circuit model is used to capture battery behaviour during usage. An equivalent circuit model using one RC-branch is used in this thesis as in Figure 1.1. This is deemed sufficient for capturing the general dynamics needed for the state of health calculations. In Figure 1.3 the voltage response for a cell is shown with the blue case being simulated values and the black dash dotted line being experimental values. The figure is taken from [6] using the model and data which it provides. It shows how the voltage and state of charge responds to a certain current cycle, here in the form of short discharge pulses. This is then expanded upon in this thesis to incorporate state of health calculations.
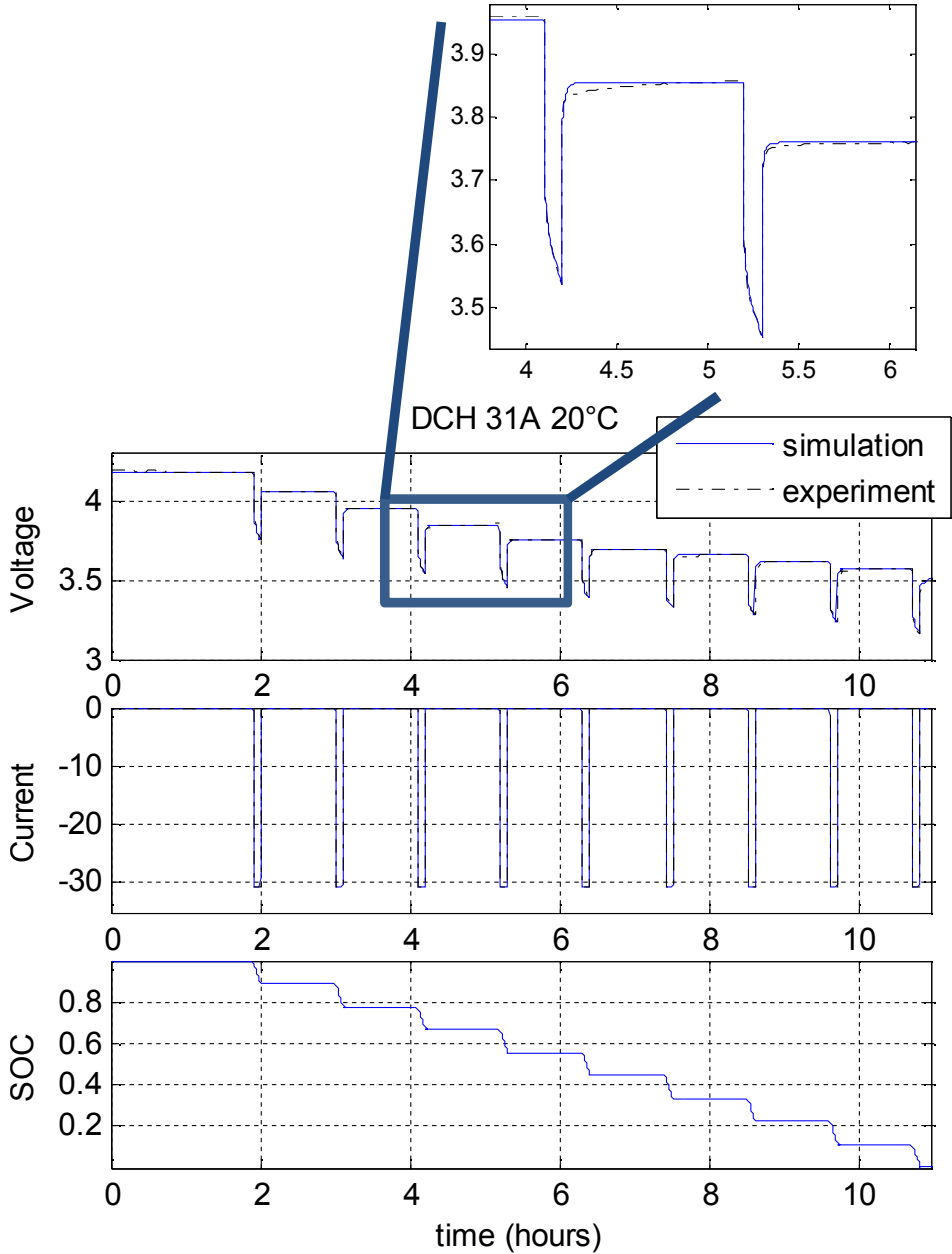
Figure 1.3: Voltage response for experimental and simulated discharges [6]

To show the effects of the different elements in a circuit model, Figure 1.4 is presented. The graph is taken from [7] and E_m is the equivalent of V_{OC}. State of charge levels SOC_a and SOC_b are before and after a discharge pulse. It is seen that the open circuit voltage converges to a new level after the discharge pulse,

with state of charge level SOC_b. There is an instant drop as well as an instant rise in voltage, R_0, when the pulse is initiated and disabled respectively. Transient behaviour is present during and after the pulse, referred to as R-C transients in the figure.
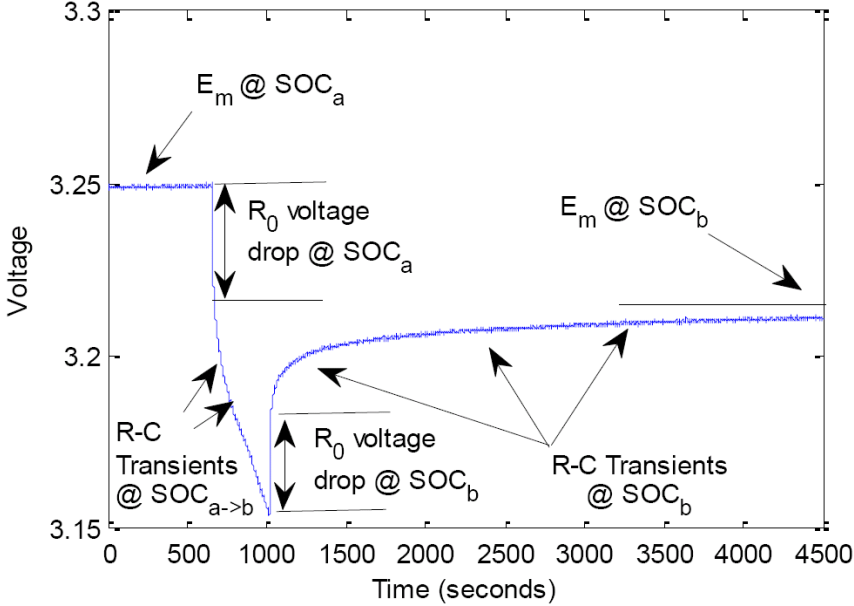
Figure 1.4: Voltage response for one discharge of a Li-Ion battery cell when going from state of charge and voltage level a to b [7]

The state of charge level is calculated through coulomb counting where the current is integrated to compute extracted charge Q_e

$$Q_e(t) = \int_0^t I(\tau)d\tau. \tag{1.3}$$

By using this, state of charge can then be calculated as

$$SoC = 1 - \frac{Q_e}{Q_{nom}} \tag{1.4}$$

where Q_{nom} is the nominal capacity of a cell. Coulomb counting is a simple technique which is not flawless. Measurement errors accumulate over time and potential parasitic reactions are not taken into account. In this thesis it is assumed that these errors do not occur and coulomb counting is considered sufficient.

The charge and discharge rate of a battery cell is often described as C-rate. This is used as a measure of a charge or discharge current in relation to the nominal capacity of the cell. A C-rate of 1 C relates to a discharge current that will

discharge a fully charged cell in one hour, i.e. a discharge rate of N C will drain a battery in $1/N$ hours.

1.2.3   State of health modelling

The state of health of a battery is an ambiguous term which may differ depending on author or usage. Long Lam, the author of [9] which presents a circuit based Li-Ion battery model, has also written a paper on capacity fading for LiFePO$_4$ cells in which he proposes a cell SoH estimation in the form of capacity loss as a function of temperature and SoC [8]. Lam claims that the C-rates for typical EV use does not affect ageing at room temperature and thus is not an input to the SoH estimation. This is tested by cycling cells with different C-rates while keeping their temperatures at the same level, proving that the temperature rise caused by ohmic heating outweigh the influence of C-rate itself. This should stay true for BEV as well as PHEV usage as long the C-rate is within the specified thresholds of the battery manufacturer. He does state that a high C-rate increases battery degradation at low temperatures. This is not modelled in his paper due to lack of experimental data and the assumption that the BMS in an EV would manage this.

Modelling capacity fade as a function of processed charge rather than cycles has advantages. Degradation is found to be affected by where in the SoC window the cell is charged or discharged, the model proposed from [8] takes this into account.

A cell also degrades over time, which is known as calendar ageing. Calendar ageing is described to a lesser extent in literature than ageing due to cycling, mainly since calendar ageing tests take several years to complete. Calendar ageing is often described solely by an Arrhenius equation which assumes constant temperature and state of charge. In [4] an ageing model which is based on the Arrhenius equation is presented but which also accounts for varying operating conditions over time. This is the model which is used in this thesis and is presented in section 2.4.

1.2.4   Pack modelling

When combining battery cells to packs there will be extra layers of complexity. In Figure 1.5 a pack of nine cylindrical cells is shown. As they dissipate heat they will influence each others temperatures. The cell in the middle is likely to be subject to the highest cell temperature as long as the ambient temperature is not higher than the cell temperatures. Temperature affects ageing and if the cells are to degrade evenly they will need to be managed with respect to this.
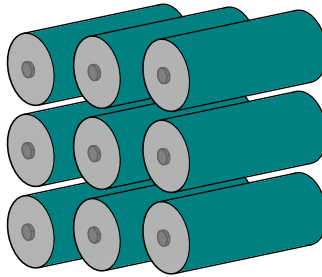
Figure 1.5: Cylindrical cells in a small pack

How the state of health is affected when the cells are combined to packs of cells is discussed in chapter 3.

1.3   Cell operation

A Li-Ion battery cell uses lithium ions to store energy. As with all batteries the function of the cell is to convert chemical energy to electrical energy, and since it is a secondary cell, also the reverse. A cell consist of a negative electrode, a positive electrode, electrolyte, and in most Li-Ion cells also a separator. The positive electrode defines what type of Li-Ion cell it is, e.g. lithium iron phosphate or lithium cobalt oxide. The negative electrode is generally made of graphite. The separator has to be porous so that lithium ions can transit between the electrodes but not the electrons.

A basic overview of battery cell operation during charging and discharging is shown in Figure 1.6. The battery cell shown in the left figure is connected to an external load and electrons flow from anode to cathode. Similarly, the flow is reversed when charging the cell as in the right figure. The anode and cathode have switched positions between the two figures as the anode by definition is the electrode at which oxidation occurs and the cathode the one where reduction occurs [11].
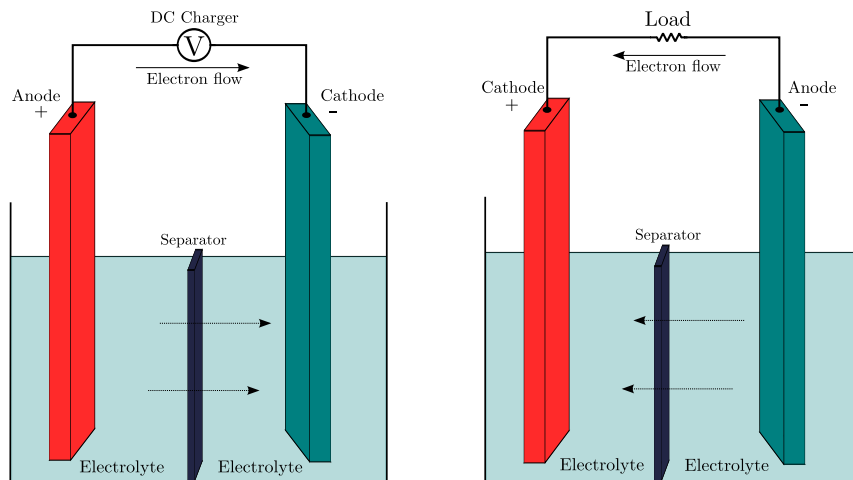
Figure 1.6: *Electrochemical operation of a battery cell during charging and discharging*

1.4   Safety concerns

Ultimately abuse of Li-Ion batteries can lead to thermal runaway and depending on battery chemistry and safety functions the result can be hazardous. Thermal management and safety procedures are important as too high temperatures can start positive temperature feedback which can initiate thermal runaway. When temperature rises too high in a cell the solid electrolyte interface breaks down and exposes the positive electrode to the electrolyte, likewise as when it first formed. This process will be in a less controlled state due to the high temperature. The reactions are also exothermic resulting in previously mentioned temperature feedback.

Further increase in temperature leads to the breakdown of electrolyte components increasing pressure within the cell. Larger cells found in vehicles typically feature safety vents to prevent explosions in this state. Furthermore the separator may melt when exposed to high temperatures leading to the short-circuiting of the anode and cathode. If the negative electrode should break down as well, then oxygen will be released, enabling fire.

The likelihood of failure varies with cell chemistry. Lithium iron phosphate batteries which seem to gain in popularity are considered to be safer than many other chemistries, as the oxygen is more strongly bounded to the iron and phosphate than it is in for instance cobalt, which is common in Li-Ion batteries.

There have been reports of Li-Ion battery failures under different circumstances. Some of the most known include consumer grade electronics such as cell phones catching fire and the Boeing 787 Dreamliner battery fire which lead to the grounding of the entire fleet of aircrafts for several months. At least one of the incidents which lead to the groundings were battery thermal runaway in Li-Ion batteries of lithium cobalt oxide type.

1.5   Outline

Chapter two covers cell degradation modelling for a single cell. Cycling and calendar ageing are covered in separate sections and the various factors that affect ageing are covered individually.

In chapter three the cell model is expanded to pack level. State of health is discussed in a broader perspective as the pack state of health will be dependant on state of health level for the individual cell and in which configuration they are connected.

The fourth chapter puts the degradation model into application to try and give an insight as to how a battery would perform in real life operation.

Chapter five summarizes the thesis and presents conclusions drawn from the work. A section about future work is also presented.

2

Cell degradation

This chapter aims to describe and model ageing of a battery cell. The mechanisms that contribute to degradation of a cell and which factors that may be relevant are explained. Ageing of a cell is divided into losses that occur during usage and storage, referred to as cycling losses and calendar losses respectively.

2.1   Ageing mechanism

Degradation and capacity fade in lithium-ion batteries are generally attributed to the growth of the solid electrolyte interface (SEI). The solid electrolyte interface is created due to reactions between the electrodes and the electrolyte. These reactions form a film which hinders lithium ions from reacting with the electrodes and as this film grows in thickness the cell degrades. Though SEI is the main contributor to cell degradation, the film is also necessary for the battery to operate as it prevents further parasitic reactions between the electrode and the electrolyte.

The growth of the SEI is dependent on how the battery is used. High temperatures as well as high states of charge contribute to the formation of the film. The SEI growth is generally attributed to the carbon electrode in a Li-Ion cell, though similar phenomena has been observed for the lithium metal oxide side as well. The chemical reactions leading to the formation of the SEI reduce the available supply of lithium ions, i.e. loss of active material, thus decreasing cell capacity. In Figure 2.1 the negative electrode is shown similar as to Figure 1.6. The yellow pellets on the electrode illustrates the SEI formation on the electrode, and show how the growth of the layer hinders reactions between electrode and ions in the electrolyte.

Electrode

Separator

SEI
layer

Electrolyte
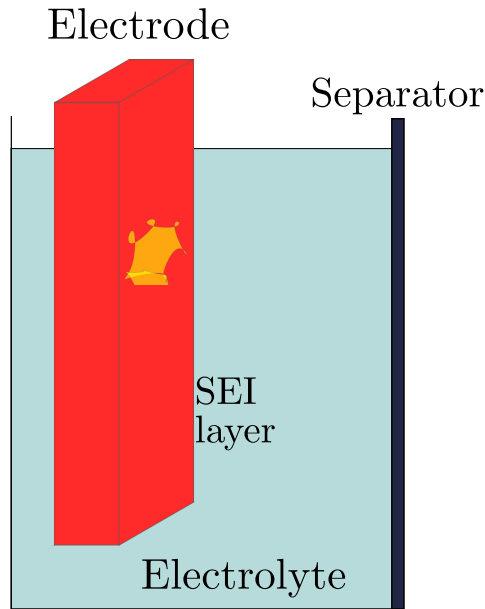
Figure 2.1: *SEI layer formation illustrated in yellow*

Other degradation mechanisms than SEI growth occur in a Li-Ion cell though these are not described in the literature to the same extent as the SEI. One such mechanism is lithium plating which generally occurs due to overcharging of the cell. If the graphite electrode can not accommodate lithium ions they may accumulate on the surface of the electrode as metallic lithium resulting in less free lithium ions and capacity loss. Lithium plating is also observed if a battery cell is operated in too low temperatures. Plating on the electrode is dendritic and may eventually lead to short-circuiting of the electrodes.

Lithium plating may also occur during fast charging of a battery. Intercalation is the insertion of molecules into a layered structure, in this case graphite. If the intercalation of lithium ions on the anode do not happen quickly enough lithium plating may occur, similar to the situation with overcharge. This problem can be avoided by charging the battery with high current pulses instead of constant current [10]. This is possible since the lithium ions spread out and dissipate into the electrolyte interface during the resting periods between the pulses, thus avoiding overpotential and lithium plating.

The degradation modelling does not take factors such as overcharge, overdischarge or usage of the battery in extreme high or low temperatures into account. Overcharge and overdischarge is when a cell is charged or discharged outside of its cut-off voltages. In this thesis it is assumed that there is no such abuse of the battery cell as described above, as this should generally be handled by a BMS in a vehicle.

2.2   State of health

The state of health of a battery cell is a figure of merit of how much the battery is degraded compared to its nominal state. By convention the end of life criteria is set to when the capacity of the battery has degraded to 80 % of its original value. The definition of state of health is somewhat arbitrary and may vary upon application but in the EV application the 80 % limit is generally used. A battery cell also experience power loss as the internal resistance of a cell increases when the battery deteriorates. This may be a more significant factor to determine state of health for a battery used in HEV application but is not described in literature to the same extent as capacity loss.

The SoH definition used in this thesis work is

$$SoH = \left(1 - \frac{\xi_{tot}}{0.2Q_{nom}}\right) \tag{2.1}$$

with the nominal capacity of the cell Q_{nom} and where ξ_{tot} is capacity loss due to cycling and calendar losses, which will be described further in sections 2.3 and 2.4.

Note that the state of health value will not give a fair assessment of the end of life of a battery as the degradation is not linear. The SoH parameter gives an estimation of the remaining capacity and may not be accurate as to how much longer the cell will last assuming operating conditions remain unchanged.

Cycling and calendar losses are assumed additive and thus the total capacity loss ξ_{tot} will be the sum of cycling losses, ξ_{cyc} and calendar losses ξ_{cal} as

$$\xi_{tot} = \xi_{cyc} + \xi_{cal}. \tag{2.2}$$

The two influencing factors are modelled individually but they both contribute to the growth of the SEI layer. It is likely that the losses are not independent as in the equation above but in the literature they are studied individually and therefore it is hard to anticipate to which extent they relate. It is reasonable to assume that ξ_{tot} would be somewhat pessimistic in this regard as cycling losses should take over capacity fading during usage of a cell and calendar losses could then be omitted.

2.3   Cycle ageing

Capacity fade due to cycling is modelled as a sum of events where factors affecting ageing are constant within the individual event i. To model thermal degradation the Arrhenius equation is used along with an empirical coefficient. The Arrhenius equation uses cell temperature T and reference temperature T_{ref}, activation energy E_a and the gas constant R. Reference temperature T_{ref} is the temperature to which the cells are brought back to after cycling to measure capacity fade and is 25° C. The empirical coefficient paired with it uses model parameters

k_{sn}, state of charge average SoC_{avg} over event i and state of charge normalized deviation SoC_{dev} from SoC_{avg}. The activation energy E_a is an experimentally determined parameter indicating sensitivity of a chemical reaction related to temperature, whose value is provided with the equation. The equation for determining capacity fade due to cycling, ξ_{cyc}, is computed as

$$\xi_{cyc}\left(T, SoC_{avg}, SoC_{dev}, Q_{proc}\right) =$$
$$\sum_i^E \left(k_{s1} SoC_{dev,i} e^{\left(k_{s2} SoC_{avg,i}\right)} + k_{s3} e^{\left(k_{s4} SoC_{dev,i}\right)}\right) e^{\left(-\frac{E_a}{R}\left(\frac{1}{T_i} - \frac{1}{T_{ref}}\right)\right)} Q_{proc,i}. \quad (2.3)$$

An event is a predetermined period of time. For all simulations in this chapter an ad hoc choice of a time of 1000 seconds is used for each event to try to capture temperature and state of charge dynamics. A short event time of a few seconds increases the degradation rate in the simulations.By this method the life of a cell is divided into sections and the degradation of each section is calculated and summed up. The whole series of all such events make up the whole life so far for a single battery cell. It would be fit to make experimental tests on battery cells to assess what an adequate event time is, and also evaluate if there are better conditions than time for event triggers, such as SoC.

The parameter $SoC_{avg,m}$ is the average state of charge in an event, and is defined as

$$SoC_{avg,m} = \frac{1}{\Delta Q_{proc,m}} \int_{Q_{proc,m-1}}^{Q_{proc,m}} SoC \, dQ_{proc}. \quad (2.4)$$

In these equations $Q_{proc,m-1}$ is the initial amount of charge processed at any certain event m, $Q_{proc,m}$ is the processed charge at the end of event m and $\Delta Q_{proc,m}$ is the difference between the two.

Parameter values for cycling degradation calculations are given in Table 2.1. The parameters were given in [8] where they were estimated from data using MATLAB curve and surface fitting tools

Using this definition of average state of charge, the normalized standard deviation of state of charge, SoC_{dev}, is calculated as

$$SoC_{dev,m} = \sqrt{\frac{1}{\Delta Q_{proc,m}} \int_{Q_{proc,m-1}}^{Q_{proc,m}} (SoC - SoC_{avg,m})^2 \, dQ_{proc}}. \quad (2.5)$$

Modelling capacity fade as a function of processed charge rather than cycles has advantages. Degradation is found to be affected by where in the SoC window the cell is charged or discharged, and using the proposed model in (2.3) takes this into account.

Table 2.1: Cycling loss model parameters used in (2.3)

Parameter	Value
T_{ref}	25°C
R	8.314 J/molK
E_A	78.06 kJ/mol
k_{s1}	$-4.092 \cdot 10^{-4}$
k_{s2}	-2.167
k_{s3}	$1.408 \cdot 10^{-3}$
k_{s4}	6.130

In [8] a cell exposed to -20°C was cycled but experienced severe capacity loss. The results from that cell are not taken into account and the model is assumed invalid for sub-zero temperatures °C as other degradation effects than SEI formation occurs in such conditions, such as lithium plating.

In upcoming sections the effects of factors contributing to capacity loss due to cycling are shown. One section each for state of charge, temperature, and charge rate.

2.3.1 State of charge

To illustrate the impact state of charge has on the degradation due to cycling simulations, are done with average state of charge and state of charge deviation being the only parameters varied.

In Figure 2.2 the same cycling scheme is used for three cases but initial charge level is altered. The cell is cycled using a 0.4 C charge for one hour and a 0.4 C discharge for one hour with one hour of rest between charge and discharge periods. There is quite some difference between the cases, illustrating that a low state charge level is preferred if degradation is the only consideration. The amount of processed charge in the figure correspond to thirty days worth of cycling.
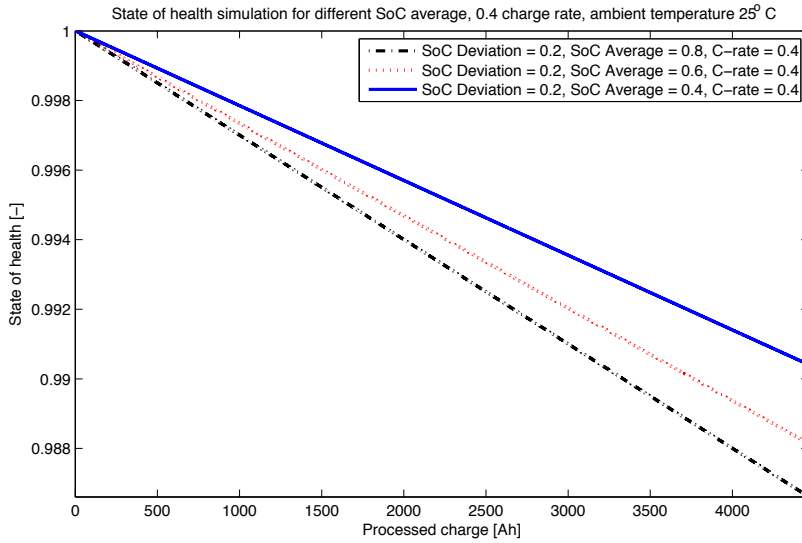
Figure 2.2: *State of health for different average state of charge*

For the state of charge deviation a similar test is conducted. The average level is kept the same for three cases but the charge rate is varied, temperature is set constant at 25° C so that the only varying factor i SoC deviation. As shown in Figure 2.3, the deviation in itself has small impact on degradation.
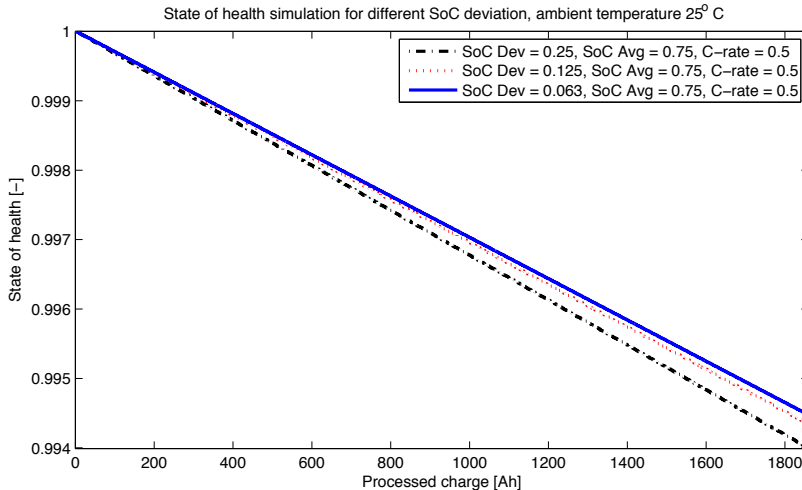
Figure 2.3: *State of health for different deviations of state of charge*

To illustrate the impact on degradation of the average state of charge and the

state of charge deviation they are plotted in Figure 2.4. Temperature and processed charge is held constant at 25° C and 1 Ah. The figure shows that high average level as well as high deviation of state of charge increases battery degradation. It should also be noted that for low SoC average and relatively high deviation the capacity fading is negative which is impossible, as the cell would gain capacity. The explanation for this is that the model is an empirical fit to experimental data which do not cover these regions. This is natural as large portions of these regions are practically impossible to operate in. Average state of charge and state of charge deviation are defined as in (2.4) and (2.5). The SoC deviation can never be higher than SoC average, e.g. if the average level is 10 % the deviation could not go above 10 % as this would increase the SoC average. Similarly the top segment of the graph is neither possible to reach as 100 % SoC average is only possible with 0 % SoC deviation.

In this figure as well as forthcoming surface plots in the cycle ageing section processed charge Q_{proc} is set to 1 Ah for simplicity.
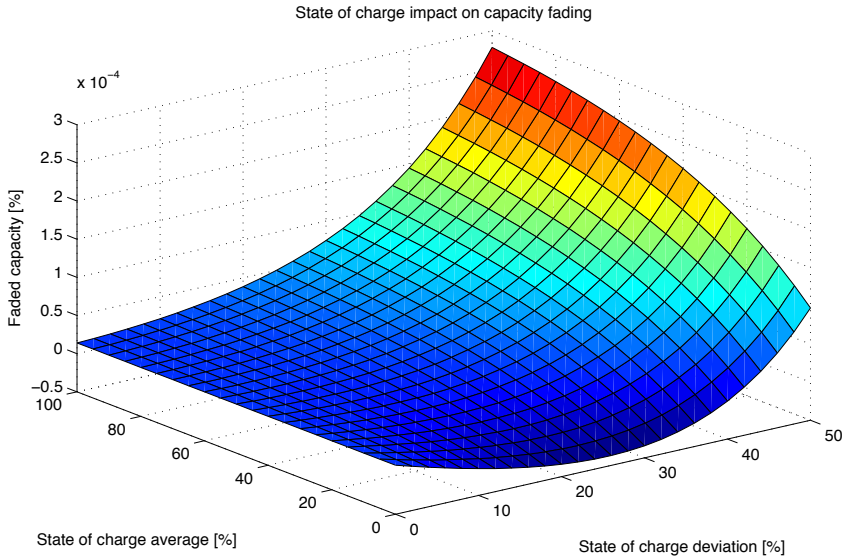
Figure 2.4: *Capacity fade as a function of SoC average and deviation*

2.3.2 Temperature

A high temperature will severely influence capacity fading. In Figure 2.5 the ambient temperature of the cell is altered and simulated using the same cycling profile. The difference between high and low temperature is significant. An increase of ambient temperature by 5°C would nearly halve the lifetime of a cell if operated as in this simulation.
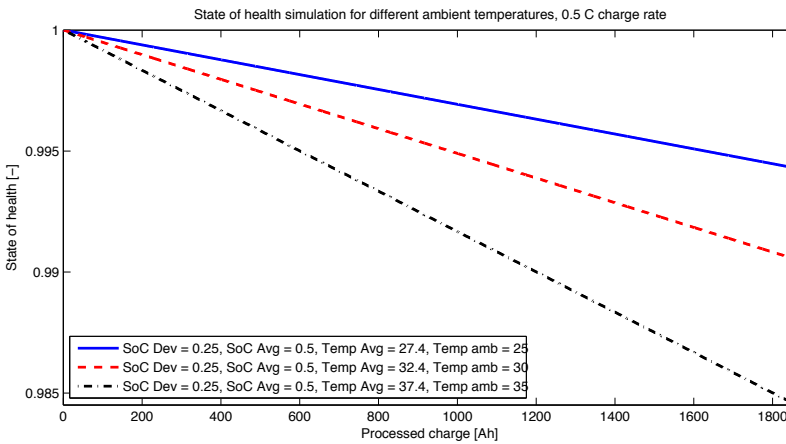
Figure 2.5: *Capacity fade for different ambient temperatures*

As with state of charge average and deviation a surface plot can illustrate the impact of temperature on degradation for each iteration by plotting the function for capacity loss due to cycling as a surface plot. This is shown in Figure 2.6 where degradation is shown against temperature and state of charge deviation. To show the degradation effect in plausible operating regions, the temperature is shown ranging from 25 °C to 50 °C and the state of charge deviation is shown from 0 % to 15 %. This figure shows that the temperature increase has a large impact on capacity fade even at low temperatures. The surface will keep the shown characteristics in ranges outside of the shown regions.
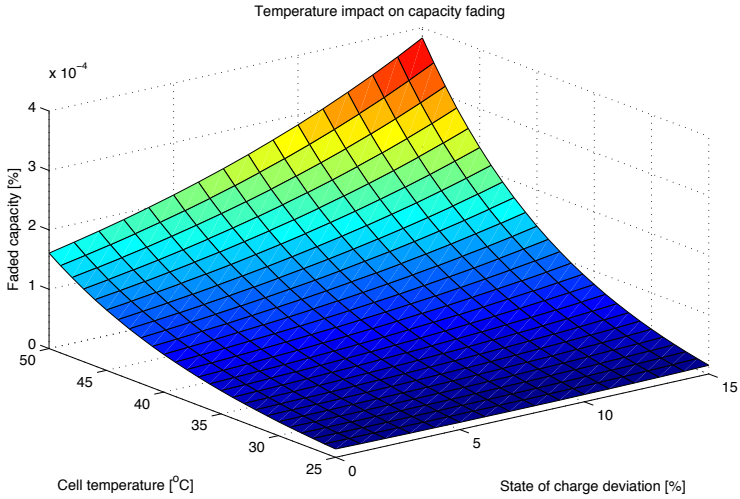
Figure 2.6: *Capacity fade as a function of temperature and SoC deviation*

The same plot is shown for temperature and average state of charge in Figure 2.7. It would seem as though the deviation is a larger factor than the average state of charge when looking at these surfaces, this is not necessarily the case. State of charge deviation will generally only be a few percent in one iteration of degradation calculation as in (2.3) and thus never reach such levels while average state of charge may vary throughout the whole operating range.
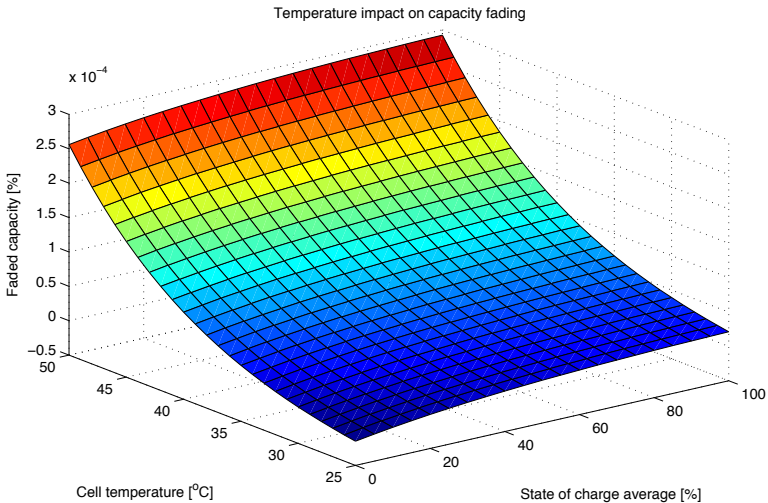
Figure 2.7: *Capacity fade as a function of temperature and SoC average*

2.3.3 Charge rate

While charge rate in itself is not a factor in the ageing model, a high charge rate will increase the temperature of a cell through ohmic heating. By conducting a test similar to the one showed in Figure 2.3 but with temperature differences taken into account the impact of the charge rate is demonstrated.

In Figure 2.8 the upper plot shows capacity fade for a cell simulated for three different charge rates. The test is set up so that processed charge is identical for the three different cases, and the lower plot shows cell temperature. An increased charge rate along with the elevated temperature associated with it strongly affects the degradation. This can be compared to Figure 2.5 where the difference between average cell temperature is roughly the same at close to 5°C as if compared to the 1 C-rate and 2 C-rate cases in Figure 2.8. The higher peak temperature increase degradation severely.
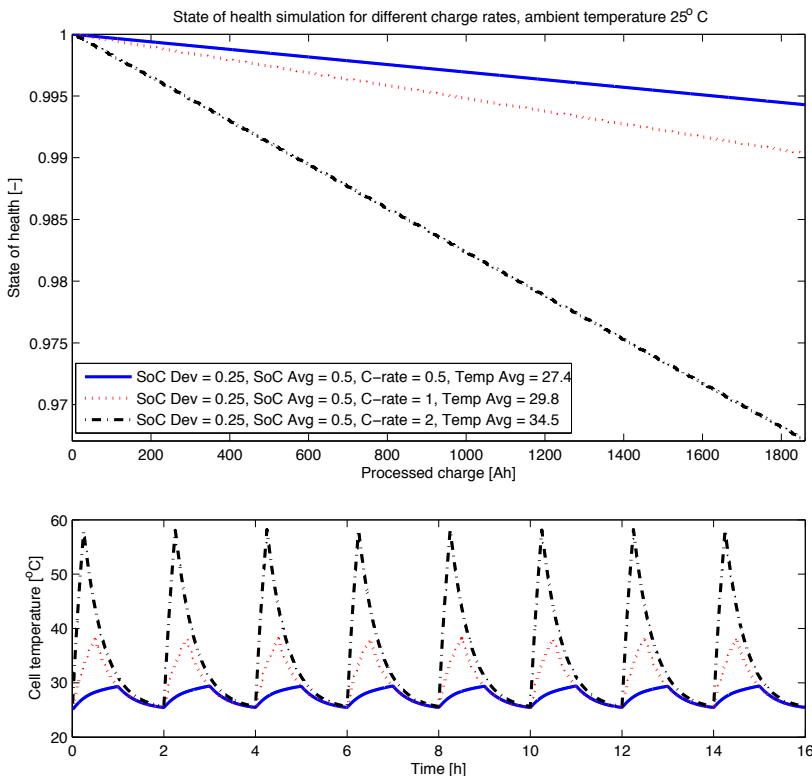
Figure 2.8: *Capacity fade with varying rates of charge*

2.4 Calendar ageing

Calendar capacity losses are modelled as a function of time, temperature and state of charge. Models predicting capacity loss of a battery during storage often only take temperature into consideration and also assume constant operating conditions. For a battery in EV application this will not be true, both the state of charge level and the temperature are likely to vary. The model implemented in this thesis considers degradation rate which allows prediction of capacity loss during varying operating conditions.

The model for calendar ageing employs Arrhenius equations to describe how calendar loss is affected by temperature and an empirically determined relationship for state of charge. A $k\sqrt{t}$ relationship for time is often used when describing calendar ageing of batteries. This is found to be insufficiently accurate in [4]. To compensate this a parameter α is introduced which is dependent on temperature. The parameter $\alpha(T)$ was determined in [4] from experimental data using non-linear regression and implemented in this thesis in Simulink as a one dimensional lookup table. Values for $\alpha(T)$ for three temperatures are given in Table 2.2.

Table 2.2: Values of the parameter α

Temperature	α
$30°C$	3
$45°C$	3
$60°C$	7

The equation for calendar capacity loss ξ_{cal} at the time t is

$$\frac{d\xi_{cal}}{dt} = k(T, SoC)\left(1 + \frac{\xi_{cal}(t)}{Q_{nom}}\right)^{-\alpha(T)} \tag{2.6}$$

with Q_{nom} as nominal cell capacity and α as described earlier. Here $k(T, SoC)$ describes the kinetic dependence of capacity fade based on temperature and state of charge.

The kinetic dependence $k(T, SoC)$ is computed as

$$k(T, SoC) = k_A e^{\frac{-E_A}{R}\left(\frac{1}{T} - \frac{1}{T_{ref}}\right)} SoC + k_B e^{\frac{-E_B}{R}\left(\frac{1}{T} - \frac{1}{T_{ref}}\right)} \tag{2.7}$$

where the parameters E_A and E_B are experimentally determined activation energies in Arrhenius equations and k_A and k_B are model parameters. The ideal gas constant R is used as with cycle ageing and so is also cell temperature T and reference temperature T_{ref}.

It can be seen in equation (2.7) that $k(T, SoC)$ has an exponential relationship to temperature and varies linearly with state of charge. The parameters are

estimated using non-linear regression and are shown in Table 2.3. As there is a multiplication of SoC and an Arrhenius equation, a high state of charge will increase the effect that high temperature has on degradation and vice versa.

Table 2.3: Calendar loss model parameters

Parameter	Value
k_A	$4.39 \cdot 10^{-5}$
E_A	182 kJ/mol
k_B	$1.01 \cdot 10^{-3}$
E_B	52.1 kJ/mol

To show the impact of each factor during calendar ageing surface plots can be made as in the section on cycle ageing. If temperature and state of charge are assumed constant, which makes $k(T, SoC)$ constant, (2.6) can be integrated and rewritten as

$$\xi_{cal} = Q_{nom} \left(\left(\frac{k(T, SoC)(1 + \alpha(T))t}{Q_{nom}} + 1 \right)^{\frac{1}{1 + \alpha(T)}} - 1 \right) \tag{2.8}$$

assuming no initial capacity loss and time $t = 0$.

This is shown by taking the derivative of (2.8), shown as

$$
\begin{aligned}
\frac{d\xi_{cal}}{dt} &= \frac{d}{dt} \left(Q_{nom} \left(\left(\frac{k(T, SoC)(1 + \alpha(T))t}{Q_{nom}} + 1 \right)^{\frac{1}{1 + \alpha(T)}} - 1 \right) \right) \\
&= \frac{Q_{nom}}{1 + \alpha(T)} \frac{k(T, SoC)(1 + \alpha(T))}{Q_{nom}} \left(\frac{k(T, SoC)(1 + \alpha(T))t}{Q_{nom}} + 1 \right)^{\frac{1}{1 + \alpha(T)} - 1} \\
&= k(T, SoC) \left(\frac{k(T, SoC)(1 + \alpha(T))t}{Q_{nom}} + 1 \right)^{\frac{-\alpha(T)}{1 + \alpha(T)}} \\
&= k(T, SoC) \left(\left(\frac{k(T, SoC)(1 + \alpha(T))t}{Q_{nom}} + 1 \right)^{\frac{1}{1 + \alpha(T)}} \right)^{-\alpha(T)} \\
&= k(T, SoC) \left(1 + \frac{\xi_{cal}}{Q_{nom}} \right)^{-\alpha(T)}
\end{aligned}
\tag{2.9}
$$

which results in (2.6).

By using (2.8) a surface plot can be generated for varying temperatures and states of charge. To consider $\alpha(T)$, cubic interpolation is used which is shown in Figure 2.9 with values as specified in Table 2.2 marked with crosses. This differs somewhat from the Simulink implementation of a 1D lookup table which

assumes linear evolution for temperatures higher than 45 °C but they should both give similar results for the simulated range.
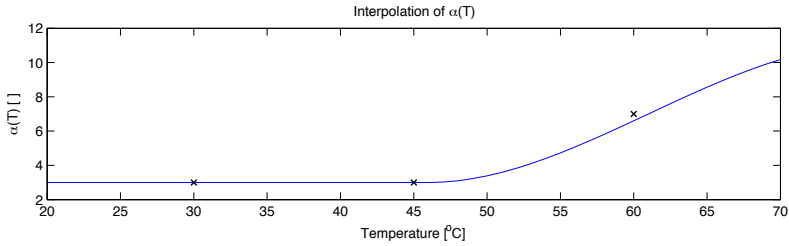
Figure 2.9: Interpolated values of $\alpha(T)$ used in surface plots

In Figure 2.10 a surface plot is shown for the whole state of charge range and temperatures ranging from 20 °C to 40 °C. The capacity loss is shown on the z axis and corresponds to one day's worth of degradation when exposed to temperature and state of charge as specified on the x and y axes. This figure shows that high temperature along with high state of charge increases calendar ageing. It also displays the linearity of the state of charge influence and exponential relationship to temperature as seen in (2.7). One can see more than a triple increase in degradation when comparing 20 °C to 40 °C.
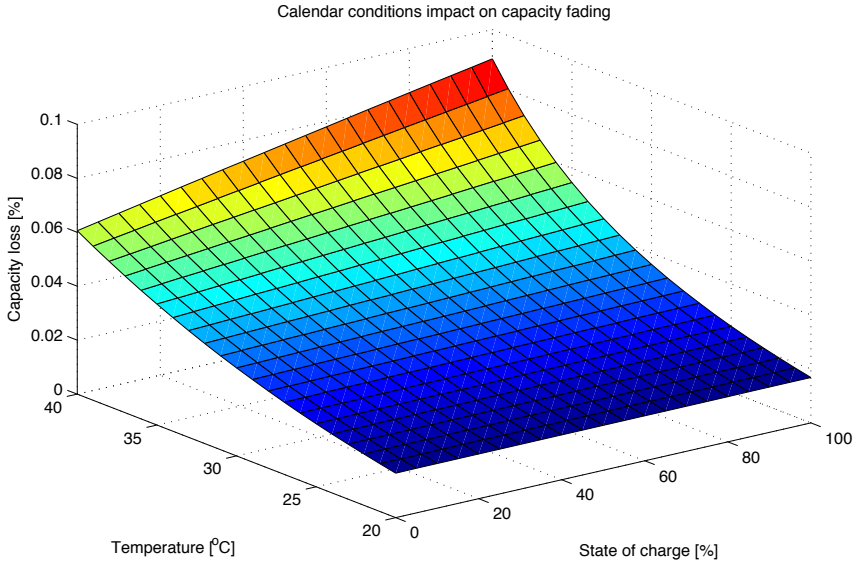
Figure 2.10: Surface plot for calendar capacity loss

By simulating the battery model in Simulink without any current running through the cell, calendar losses can be simulated for different operating con-

ditions with time taken into consideration. This is done for different ambient temperatures in Figure 2.11, where the state of charge is initially set to 50 % in all cases. One can see that temperature has severe influence on degradation. A cell exposed to 35°C as compared to 25°C will degrade to 0 % SoH in nearly half the time. It is also worth noting that the degradation rate declines with time.
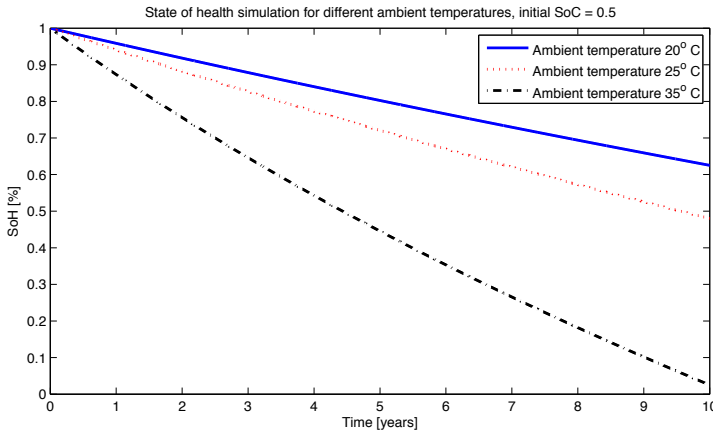
Figure 2.11: Calendar losses for different ambient temperatures

The same test is performed but for different states of charge with temperature set to 35°C and shown in Figure 2.12. The time span is somewhat shorter than in the previous figure. It is clear that the state of charge has a smaller impact on the state of health than temperature but different levels of state of charge would still affect the longevity of a cell by some years.
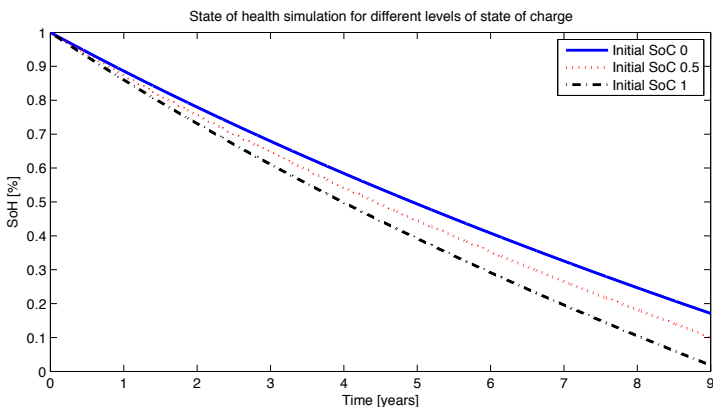
Figure 2.12: Calendar losses for different initial states of charge

2.5   **Summing up**

The results of cycle ageing along with calendar ageing during usage are presented in more realistic scenarios in chapter 4. To show the characteristics of degradation for calendar losses together with cycling losses Figure 2.13 is presented below for a period of fourteen days as well as a year.
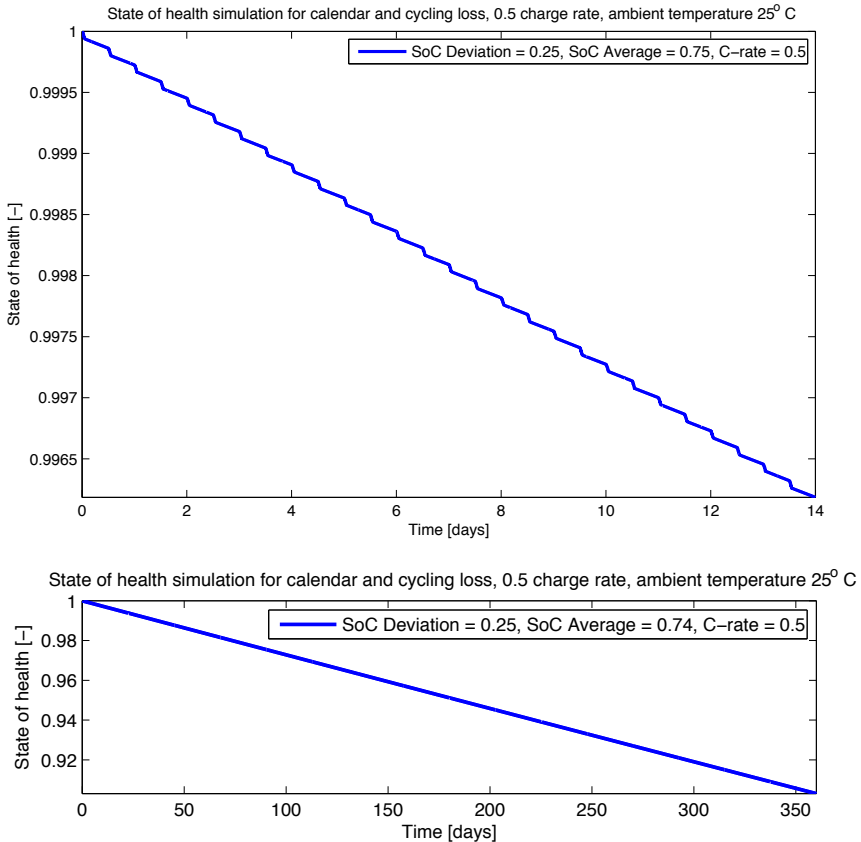
Figure 2.13: *Calendar and cycling losses combined*

The cell here is exposed to one hour of 0.5 C discharge followed by 11 hours of rest, then one hour of 0.5 C charge and 11 hours of rest which repeats for some time. It is seen that the cell is degrading almost linearly during the resting periods with increasing slopes during the charge and discharge periods. The whole process can be seen as linear as the scheme is repeating itself. Should the sequence be simulated for long enough time the non linear calendar loss relation to time would be seen.

There is also a feedback effect to degradation which is not depicted well in the figures so far. As the cell degrade and loses capacity the charge rate needed

to process a certain amount of charge will be higher as the capacity of a cell will decrease from its nominal value. This leads to higher temperature and produces something of a vicious circle. The effects of cycling losses and calendar losses for long periods of time can be summarized as cycling losses will increase during the lifetime of a cell and calendar losses will decrease with time.

3

Pack degradation

When extending the state of health modeling from cell to pack level, the complexity increases. The cells will exchange heat with each other and a definition of the pack state of health needs to be made. This is discussed in this chapter.

3.1 Pack balancing

If battery cells are put together in a pack they will be subject to different stress conditions. As the cells are not identical and the current drawn may not be exactly the same, the cells will not have the same state of charge level. To account for this the cells will need to be balanced. This may be done either actively by transferring energy from cells with high charge to cells with low, which requires a sophisticated BMS, or by just limiting a series of cells to the capacity of the weakest cell in the series. In this thesis there are no balancing circuits implemented so the state of health calculation will always be based on the lowest cell in a serial connection.

3.2 Pack state of health

For cells that are connected in series, the voltage of the circuit will add up and capacity remains the same as the individual cells. When connected in parallel the capacity of the cells add up while the voltage remains the same as of one individual cell. In Figure 3.1 four battery cells are displayed in serial and parallel circuits.
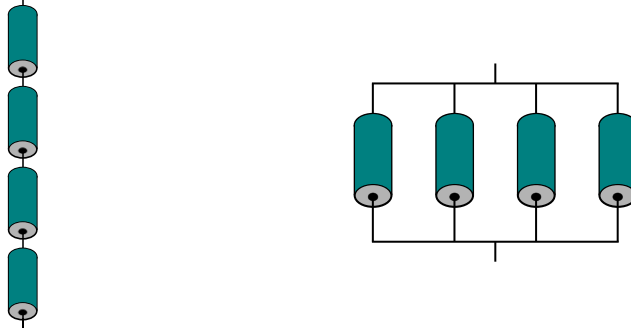
Figure 3.1: *Cells connected in serial (left) and parallel (right) configuration*

For a series of cells the capacity will be limited to the capacity of the lowest cell in the string. This is assuming that there is no active equalization of the cells, i.e. energy is not transferred to a cell with low capacity from a cell with high capacity. For a series connection of n_i cells, the capacity of the series, Q_{series}, is the capacity of the cell with the lowest capacity, as

$$Q_{series} = \min_i(Q_i) \quad i \in \mathbb{Z}^+ , \ i \leq n_i \tag{3.1}$$

where i denotes each individual cell.

If cells are connected in parallel the capacity adds up to the sum of the individual cells capacity as

$$Q_{parallel} = \sum_{j=1}^{n_j} Q_j. \tag{3.2}$$

Here $Q_{parallel}$ is the capacity for the parallel circuit, j denotes the individual cells, and n_j is the total number of cells.

As the state of health of a battery cell is based on the capacity of the cell, the state of health of a pack will be based on the capacity of the cells the pack consist of. In a series circuit the pack SoH will be the minimal SoH of the series, as

$$SoH_{series} = \min_i(SoH_i). \tag{3.3}$$

In a parallel circuit the pack SoH will be the average SoH of the cells, as

$$SoH_{parallel} = \frac{1}{n_j} \sum_{j=1}^{n_j} SoH_j. \tag{3.4}$$

When several cells are connected in series and parallel circuits there are two different configurations available. A pack consisting of one parallel connection with several series connections is known as a parallel-serial connection (PS). Likewise a circuit with several parallel connections in one series is known as a serial-parallel connection (SP). The two configurations are shown in Figure 3.2. These configurations would have the same nominal capacity and voltage.
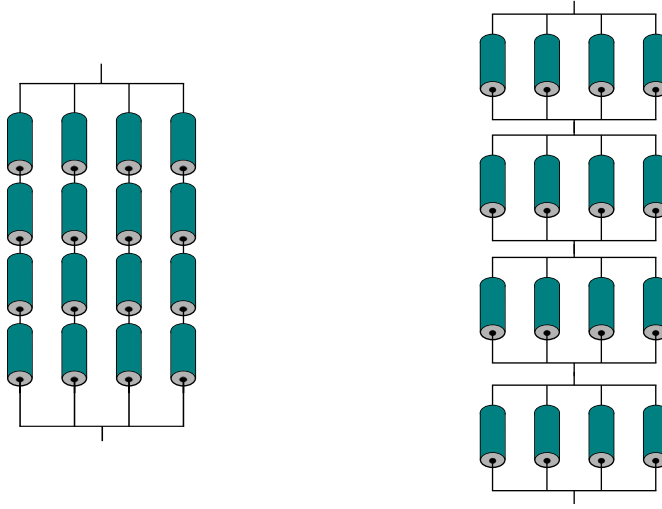
Figure 3.2: *Parallel-serial (left) and serial-parallel (right) configurations of cells*

The state of health for these types of circuits are derived from (3.3) and (3.4), and thus computed as

$$
SoH = \begin{cases} \dfrac{1}{n_j} \displaystyle\sum_{j=1}^{n_j} \left(\min_i \left(SoH_{i,j} \right) \right) & \text{for PS,} \\[3ex] \min_i \left(\dfrac{1}{n_j} \displaystyle\sum_{j=1}^{n_j} SoH_{i,j} \right) & \text{for SP.} \end{cases} \tag{3.5}
$$

For a pack of cells that have the same capacities the pack SoH will be identical, but as the cells degrade the SoH will differ with configuration. The state of health calculation for the two cases will result in the same SoH if only one cell has degraded, or all degraded cells are in the same series and parallel connections with the same level of degradation. For two or more cells which do not fit these criteria the SoH for a PS circuit will be lower than the SOH for a SP circuit. To illustrate this four matrices representing sixteen cells as in Figure 3.2 are shown in the matrices below, where each matrix value represents the SoH of a cell in that position. This is done for a single degraded cell, five degraded cells which are aligned in serial and parallel with the same SoH, two degraded cells which are not aligned in serial or parallel, and all cells randomly assigned SoH values. There are state of health calculations for the PS and SP cases below each matrix.

$$
\begin{bmatrix} 1 & 1 & 1 & 1 \\ 1 & 0.5 & 1 & 1 \\ 1 & 1 & 1 & 1 \\ 1 & 1 & 1 & 1 \end{bmatrix}
\begin{bmatrix} 1 & 0.5 & 1 & 1 \\ 0.5 & 0.5 & 0.5 & 1 \\ 1 & 0.5 & 1 & 1 \\ 1 & 1 & 1 & 1 \end{bmatrix}
\begin{bmatrix} 1 & 1 & 1 & 1 \\ 1 & 0.5 & 1 & 1 \\ 1 & 1 & 0.5 & 1 \\ 1 & 1 & 1 & 1 \end{bmatrix}
\begin{bmatrix} 0.5 & 0.3 & 0.4 & 0.6 \\ 0.1 & 0.3 & 0.4 & 0.7 \\ 0.4 & 0.5 & 0.7 & 0.7 \\ 0.3 & 0.9 & 0.7 & 0.4 \end{bmatrix}
$$

$$
\begin{aligned}
SoH_{PS} &= 0.875 & SoH_{PS} &= 0.625 & SoH_{PS} &= 0.750 & SoH_{PS} &= 0.300 \\
SoH_{SP} &= 0.875 & SoH_{SP} &= 0.625 & SoH_{SP} &= 0.875 & SoH_{SP} &= 0.375
\end{aligned}
$$

This can be summarized as that no matter the situation an SP circuit will always have equal or higher state of health than a PS circuit.

3.3   Simulations

To show the principal behaviour of cells in a pack, simulations are done with six cells in SP and PS configuration where three cells are in series and two in parallel in the circuits. Heat exchange is modelled as convection between the cells and the environment, as well as convection between the cells as there is assumed to be a layer of air surrounding the cells. The heat exchange is governed by Newton's law of cooling

$$
\frac{dQ}{dt} = hA\left(T_a(t) - T_b(t)\right) \tag{3.6}
$$

where heat transfer is directly proportional to surface area A, heat transer coefficient h and temperature difference $T_a - T_b$, and Q is thermal energy. There is an assumption of no active cooling in the circuits simulated. Heat exchange in a pack is demonstrated in Figure 3.3, where the cells are blue and heat transfer is illustrated as orange arrows.

Figure 3.3: *Heat exchange modeling of six cells*

Simulations for packs of cells are shown for shorter periods of time than the single cell figures in chapter 3. This is because simulation time increases as the number of cells increase, roughly with a $t_n = 2n \cdot t_1$ relationship where t_n and t_1 is simulation time for n cells and one cell respectively.

The number of cells is chosen as a small number of cells that can illustrate the effect of a pack while maintaining a low enough simulation time. The heat transfer will be the same whether it is a SP or PS type circuit. The cells from [6] are used which are prismatic and the thin side surfaces influence on heat exchange is omitted. To consider manufacturing differences between cells, parameter values R_0, R_1, and C_1 are normally distributed to their nominal values with a 2 % standard deviation.

In comparison to use a single cell, the cells in a pack will be exposed to higher temperatures as they exchange heat with each other instead of the environment. The battery cells may also be exposed to heat from other components of the vehicle. In this section they are cycled using a 0.5 C rate in the same manner as explained in 2.3.1.

In Figure 3.4 the state of health of all six cells in a pack are shown as well as the state of health of a lone cell in a bold dot-dashed line. Due to the symmetric layout of the cells, as shown in Figure 3.3, the temperatures will be close to identical for some cells. This results in overlapping state of health as well. The lowest line will be the two inner cells and the middle ones the four outer cells. The lower plot shows the temperature for the cells during this cycle with the same colour coding as in the figure above.
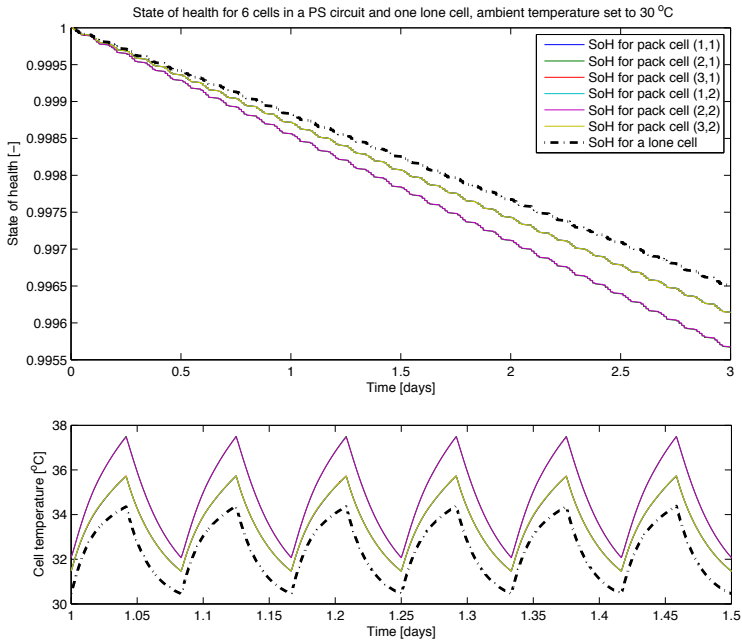
Figure 3.4: State of health and temperature for cells in a pack and a lone cell

To show the difference between parallel-serial and serial-parallel state of health calculation, one cell is given an initial 50 % SoH, as if it was faulty. Figure 3.5 shows state of health decrease in a three day simulation. It is seen that the SoH

for the PS configuration is decreasing faster than for the SP case. Both configurations start of at the same SoH, but as the other cells degrade the PS SoH will be lower as shown in the previous section.
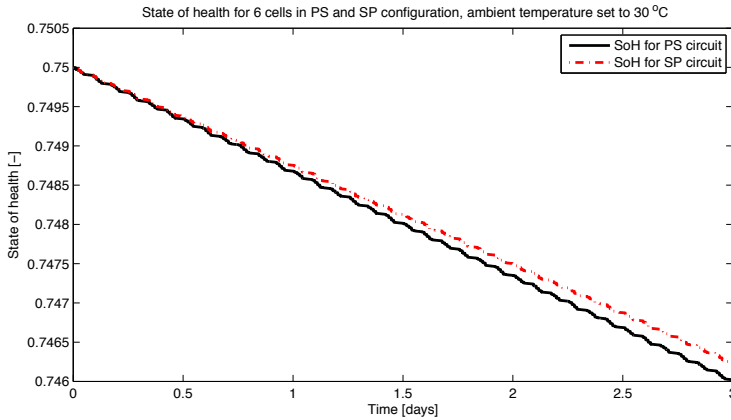
Figure 3.5: State of health comparison for PS and SP circuits

3.4   Summing up

The state of health level of a pack will in an optimal situation be the same as the state of health of a single cell's nominal value. As cells exchange heat, which is a contributing factor to battery degradation, the cells in a pack will generally degrade faster than in the case of a single cell. The opposite could occur though in a situation where battery cells are exposed to dangerously low temperatures and the heat exchange between cells would speed up the warming process. This leads to the conclusion that a sophisticated thermal management system should have a large impact on the longevity of a battery pack.

Battery cells are connected in series to provide the needed voltage of a pack and in parallel to reach high capacity. Depending on the configuration of the cells the state of health merit may differ as the cells degrade.

Due to long simulation times for packs of cells longer simulations of packs are not presented. The figures shown are meant to display the main characteristics of battery degradation in packs of cells as compared to single cells. There are more areas that could be explored and added to the degradation model regarding battery packs and such topics are discussed in chapter 5.

4

Application

In this chapter the degradation model is evaluated using driving cycles and a vehicle model. This is done to give a hint of how the battery cells would degrade in a real-life application.

4.1 Vehicle model

To achieve a realistic current profile during driving, a vehicle model and a driving cycle is used. An equation for longitudinal dynamics of a road vehicle is

$$m_v \frac{d}{dt} v(t) = F_t(t) - (F_a(t) + F_r(t) + \underbrace{F_g(t)}_{= \, 0}) \tag{4.1}$$

where the force $F_g(t)$ is gravitational force, traction force $F_t(t)$ is the force generated by the electric motor, excluding losses associated with the vehicles power train, $F_a(t)$ is aerodynamic drag, $F_r(t)$ is rolling resistance, m_v is vehicle mass mass and v is vehicle speed. Gravitational force $F_g(t)$ is omitted as the vehicle is assumed to travel on horizontal roads and is therefore set to zero in the equation. The forces in (4.1) are illustrated in Figure 4.1.
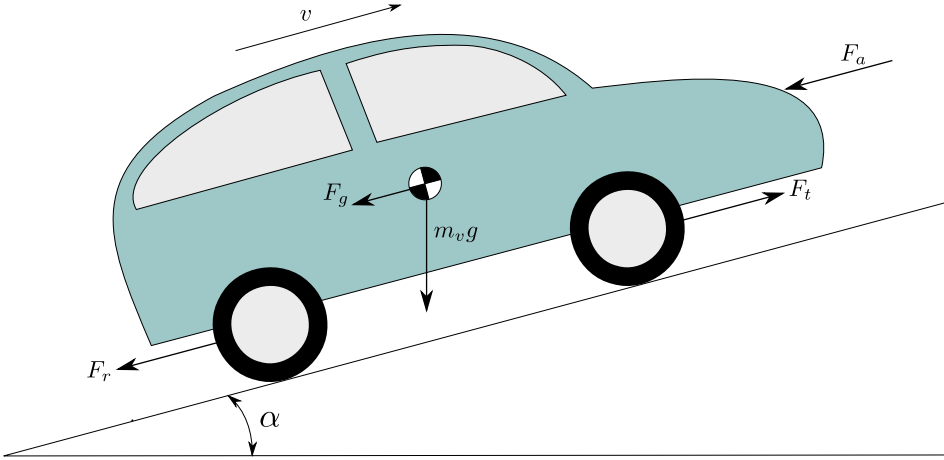
Figure 4.1: *Forces acting on a road vehicle in motion*

Aerodynamic drag, $F_a(t)$, is calculated as

$$F_a(t) = \frac{1}{2}\rho_a A_f c_d v^2 \tag{4.2}$$

where ρ_a is air density, A_f is vehicle frontal area and c_d is the aerodynamic drag coefficient.

Rolling resistance, $F_r(t)$, is

$$F_r(t) = c_r m_v g \underbrace{\cos(\alpha)}_{=\,1} \tag{4.3}$$

with m_v being the vehicle mass, g is acceleration due to gravity, c_r is the rolling resistance coefficient and α is the slope angle which is set to zero due to the assumption of a flat road.

Typical values for a normal car are assumed and used in the equations above, values for these parameters are given in Table 4.1.

Table 4.1: *Parameter values for the vehicle*

Parameter	Value	Unit
ρ_a	1.2922	kg/m^3
A_f	2.3	m^2
c_d	0.3	-
m_v	1500	kg
g	9.82	m/s^2
c_r	0.01	-
α	0	deg
η_{em}	0.85	-
η_{pe}	0.95	-

Using velocity and traction force the tractive power of a car, P_t, is calculated as

$$P_t = F_t v. \tag{4.4}$$

Power consumption for the battery, P_b can then be calculated based on P_t and the efficiency of the electric motor and the power electronics, η_{em} and η_{pe}, as

$$P_b = P_t \cdot \left(\eta_{em} \eta_{pe} \right)^{-\operatorname{sgn}(P_t)} \tag{4.5}$$

with sgn being the signum function, defined as

$$\operatorname{sgn}(x) := \begin{cases} -1 & \text{if } x < 0 \\ 0 & \text{if } x = 0 \\ 1 & \text{if } x > 0 \end{cases} \tag{4.6}$$

where x is a real number.

The power will be negative during decelerations, and this energy is used to recharge the battery through regenerative braking. The equations assume that all traction force comes from an electric motor as in an EV or a PHEV on all-electric drive.

Using the battery power consumption and battery voltage, a current profile can be derived for any given driving cycle by the definition of electrical power,

$$P_b = \frac{QV}{t} = IV. \tag{4.7}$$

For a vehicle with known parameters this means that a current profile $I_b(v, V)$ can be calculated as a function of velocity and battery voltage. This is achieved by combining (4.1) to (4.7), resulting in

$$I_b(v, V) = \frac{\left(m_v \frac{d}{dt} v(t) + \frac{1}{2} \rho_a A_f c_d v^2 + c_r m_v g \right) v}{V} \cdot \left(\eta_{em} \eta_{pe} \right)^{-\operatorname{sgn}(P_t)}. \qquad (4.8)$$

4.2   Driving cycle

A current profile is derived from a standard driving cycle using the vehicle model. The US federal test procedure driving cycle, FTP-75, is shown in the upper plot of Figure 4.2. This driving cycle is taken from real life scenarios and is presented as velocity over time. Using data for a driving cycle and equations (4.1) to (4.5), the driving cycle can be converted to a power cycle where negative sections of the power cycle are used for recharging the battery and this is shown in the lower plot of Figure 4.2.
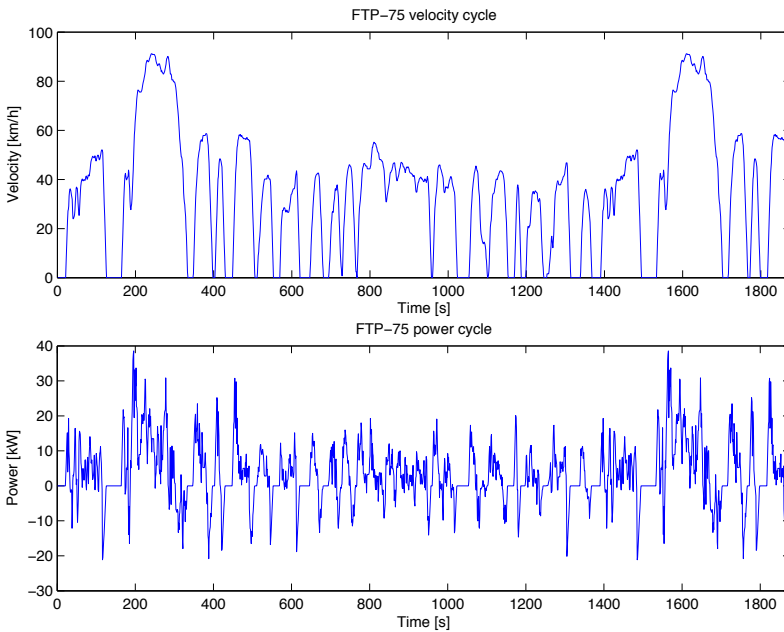
Figure 4.2: *Velocity and power consumption plot for test cycle FTP-75*

The same calculation can be done for other driving cycles as well. In Figure 4.3 the velocity and power plots are shown for the New European Driving Cycle (NEDC) which is a widely used driving cycle for certification of vehicles in Europe.
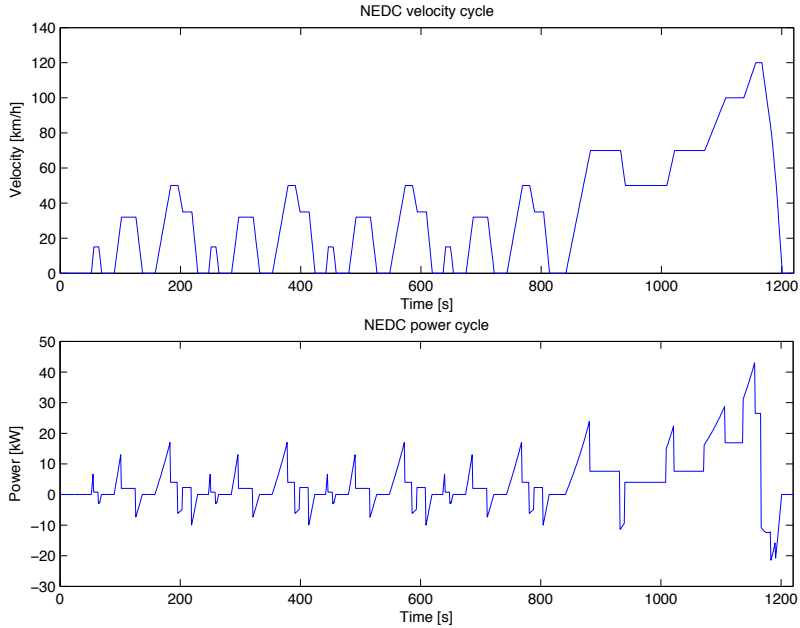
Figure 4.3: *Velocity and power consumption plot for the NEDC*

4.3   Simulations

To get a repeatable realistic test scenario a driving cycle is combined with a charging sequence. This is repeated for some time to get a state of health estimation. The power cycle needs to be converted to a current cycle using (4.7) to achieve a current profile to be used on a battery. In the upcoming test with one battery cell the current is scaled so that it gives a driving scenario with a maximum discharge peak of roughly 4 C.

One test is done with two repetitions of the FTP-75 cycle with several hours of rest in between, followed by a slow recharge. This is done for one cell over the course of a month, with an ambient temperature of 25°C and is presented in Figure 4.4. The lower plot shows how the cell's state of charge varies over one day of the cycle. As the time span is only one month, calendar ageing does not have a significant effect on degradation. The plot is essentially the same as in Figure 2.13 but for a different current cycle.

State of health simulation for different ambient temperatures
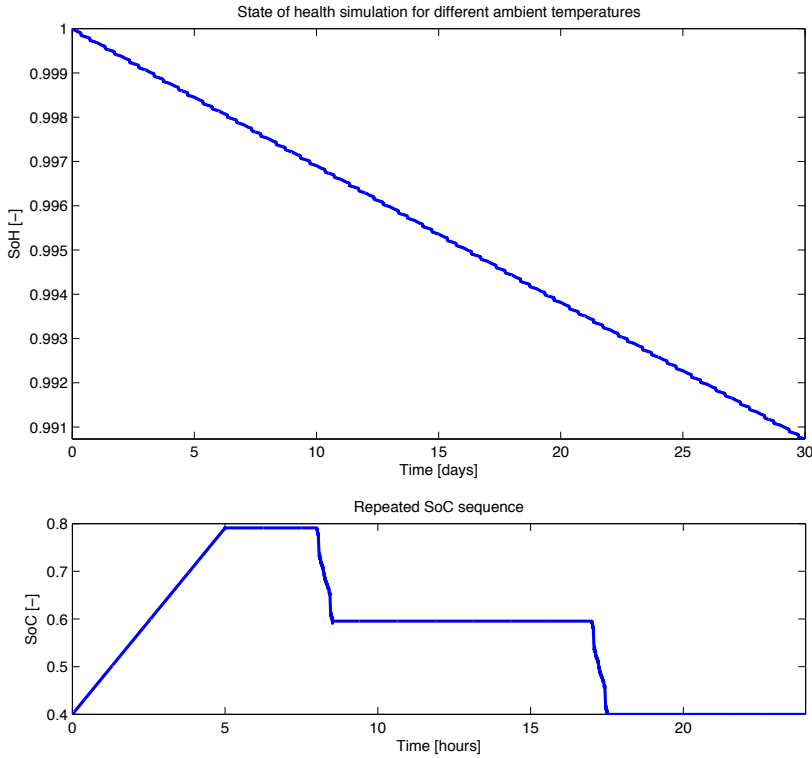
Figure 4.4: State of health and state of charge for one cell using the FTP-75 cycle

In Figure 4.5 the state of charge variation of one sequence of the FTP-75 cycle is shown.
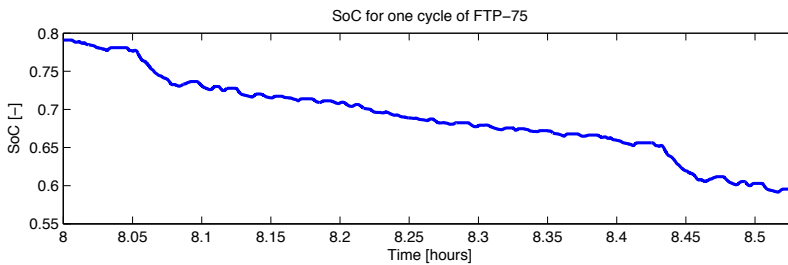
Figure 4.5: State of charge during one FTP-75 cycle

The same current sequence is used for a pack of batteries in a six cell configuration as in chapter 3, but for a shorter period of time due to increase in simulation time. This is shown in Figure 4.6. As with the case in the previous chapter the pack SoH will decrease faster than the single cell SoH due to higher

temperatures.
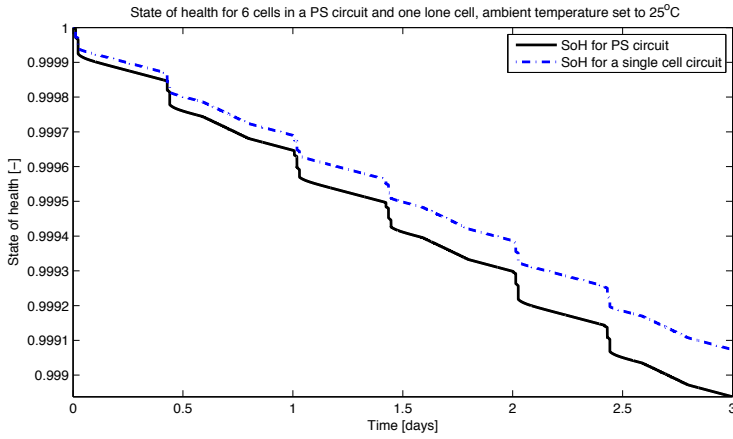
Figure 4.6: State of health for a pack and a single cell

The same test is done but for the NEDC for comparison. This is shown in Figure 4.7 where the upper plot shows the state of health and the lower plot shows the state of charge for one sequence of the driving cycle.
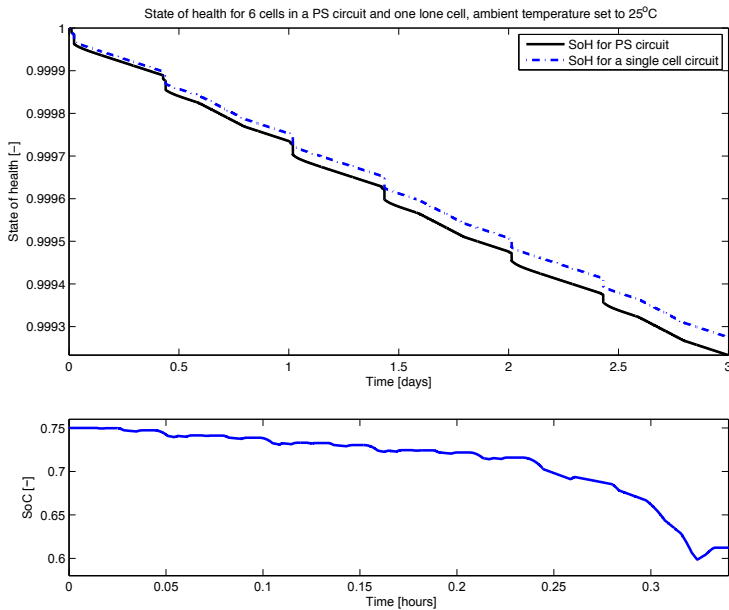
Figure 4.7: State of health and state of charge for the NEDC

A figure comparing the FTP and NEDC tests above could be made but may not

give much information on differences between the two regarding battery degradation, as the travelled distance is further in the FTP than in the NEDC.

A test is conducted for two temperatures to compare what happens in a driving cycle scenario for a battery pack under different temperatures. The pack is exposed to an ambient temperature of 25°C and 35°C. As expected, the higher temperature case degrades faster than the lower one. This is shown in Figure 4.8. Even though the figure below is mainly a confirmation of what has already been observed in the previous chapters, it functions as a good illustration of how much cycling and calendar losses could affect degradation in different climates.
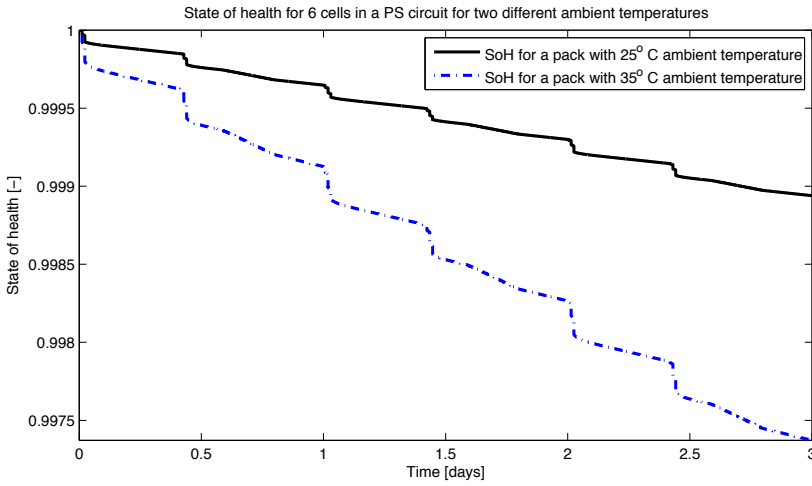
Figure 4.8: *State of health of a pack for two different ambient temperatures*

4.4 Variable temperature

This chapter aims to give an insight as how a battery pack would degrade in real life application. A plot is presented in Figure 4.9, which shows state of health, state of charge and temperature of a pack for the same current sequence as used in Figure 4.4. In Figure 4.9 the temperature is varying, following an approximation of a typical Swedish summer day with an added $T_{pe} = 5$°C temperature increase for power electronics, chosen ad hoc, $T_{avg} = 18.5$°C is the average temperature during the day and $T_{dev} = 5.5$°C is the temperature deviation during a day. The equation for the ambient temperature T_{amb} is set as

$$T_{amb}(t) = T_{avg} - T_{dev} \cdot \cos(\frac{t}{24}2\pi - \frac{3}{24}2\pi) + T_{pe} \qquad (4.9)$$

where t is time in hours.

In Figure 4.9 below, the temperature of a cell in the middle of the pack is plotted together with the ambient temperature of the pack. The state of charge

sequence is the same as in previous tests with the FTP-75 cycle, fitted over the course of the day to match a possible day of work.
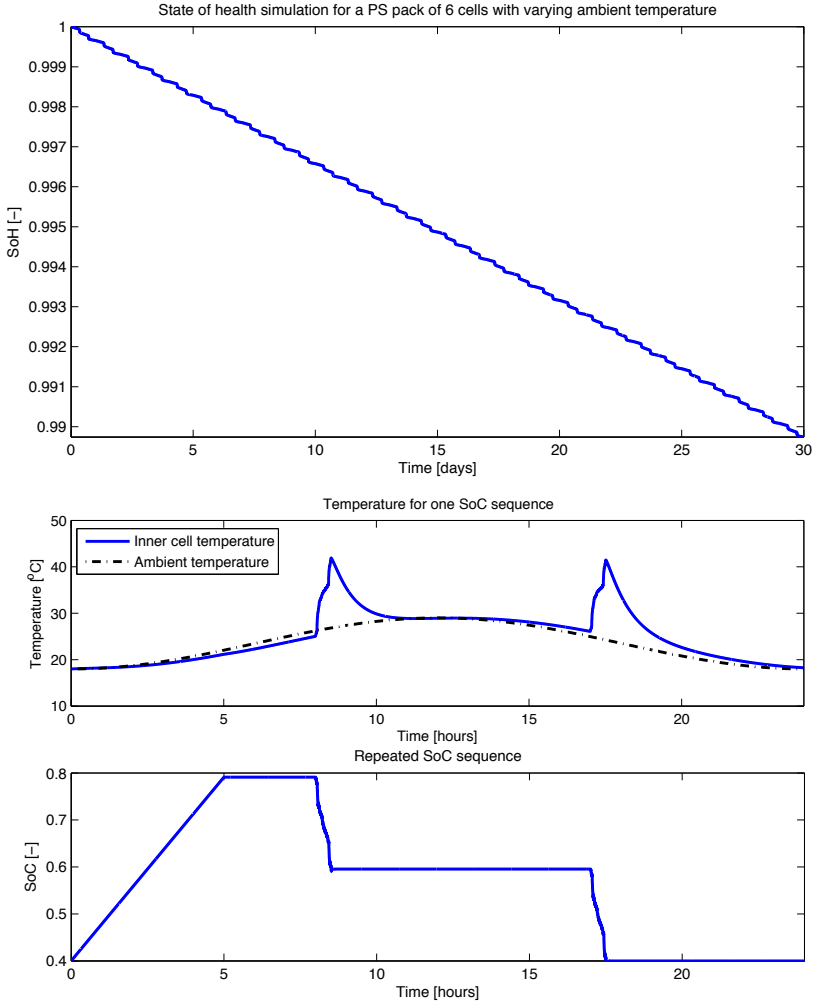
Figure 4.9: *State of health, temperature and state of charge for a pack of cells with varying ambient temperature*

4.5 Summing up

By combining the degradation models with a vehicle model and driving cycles and simulating over time, it is possible to get an assessment on the extent of degradation for a certain scenario. The same conclusions that were made for single cells and pack of cells regarding the impact of temperature and state of charge in degradation remain true. A high temperature is the most significant

factor both during usage and storage.

One can see that in the scenario used in the simulations in this chapter, cycling losses are a bigger factor than calendar losses. This relationship would be enhanced if the vehicle was driven for longer periods of time during a day, or harder in terms of more energy output from the battery during the time. However, a PHEV which is seldom charged might show an opposite relationship. If the SoC is kept at a minimum level and the electric powertrain is only used during transients it is possible that calendar ageing would play a bigger role in the degradation of the battery pack.

The simulations in this chapter are meant to give an insight into what to expect in regards to longevity of packs of cells for a given situation. The method can also help when deciding which strategies to use when designing control systems for batteries. Which can include cooling systems as well as battery management, and also possibly be a part in the decision making of when to use the electric powertrain in a hybrid vehicle.

5

Conclusions and future work

A model for Li-Ion battery cells and packs of cells that takes degradation into account has been developed. The degradation is a function of usage and time, referred to as cycle ageing and calendar ageing respectively.

The model was based on an equivalent circuit model representing a battery. This was expanded upon to also model battery degradation in the form of capacity loss. By specifying driving conditions, ambient temperature and battery cell and pack specifications it is possible to use the model for state of health assessments over time. It is possible to configure the model to match the specification of a certain battery pack in an EV and get an estimation on how the state of health is affected for a given driving scenario. As long as the power output is chosen in context to a specific vehicle the model works for BEV as well as PHEV usage.

The main conclusion that can be drawn regarding degradation is that temperature is the most influencing factor in cycle ageing as well as calendar ageing. The temperature of cells will be dependant on ambient temperature and current. State of charge level will also influence the degradation, but generally to a lesser extent than temperature.

It is better to store a lithium-ion battery with a low state of charge rather than a high level. If possible it also good to keep the state of charge low at usage with small deviations. This may not be possible for all applications, especially not for BEVs as it will impede range.

5.1   Future work

There are many things regarding degradation modeling in this thesis which could
be expanded upon. Ideally the battery cell model and ageing model data should
be of the same chemistry and specification. In this thesis the cell model is based
on lithium nickel manganese cobalt oxide cells and the ageing models are of
lithium iron phosphate type.

It would also be of interest to see if the models could be altered to decrease
simulation time and thereby be able to do longer simulations. Another issue to
consider is if it is sufficient to only consider degradation effects due to ohmic
heating for different current levels or if the current itself should be accounted for
to better model the capacity losses. This could be expanded upon to better un-
derstand differences in a degradation perspective in charging versus discharging
that are not taken into account at this moment.

The model could be extended to involve more factors that attribute to degra-
dation, such as charging above and below the cut-off voltages or the effects of
usage in sub-zero temperatures. Other areas to explore could be to include cell
balancing and a model of a battery management system. Areas which are already
covered could also be further developed, such as more detailed heat exchange,
larger battery packs and more realistic test scenarios. To be able to more easily
test different pack configurations and operating conditions it would be conve-
nient to build a graphical interface where the user could specify the information
that is wanted and let the program build and simulate the chosen scenario.

Bibliography

[1] David Andrea. *Battery Management Systems for Large Lithium-Ion Battery Packs*. Artech House, first edition, 2010. Cited on page 2.

[2] S. Bangaru, R. Alugonda, and P. Palacharla. Modeling and simulation of lithium-ion battery with hysteresis for industrial applications. In *Energy Efficient Technologies for Sustainability (ICEETS), 2013 International Conference*, April 2013. Cited on page 3.

[3] Matthieu Dubarry and Bor Yann Liaw. Development of a universal modeling tool for rechargeable lithium batteries. *Journal of Power Sources*, 174(2):856 – 860, 2007. 13th International Meeting on Lithium Batteries. Cited on page 3.

[4] Sébastien Grolleau, Arnaud Delaille, Hamid Gualous, Philippe Gyan, Renaud Revel, Julien Bernard, Eduardo Redondo-Iglesias, and Jérémy Peter. Calendar aging of commercial graphite/lifepo4 cell – predicting capacity fade under time dependent storage conditions. *Journal of Power Sources*, 255(0):450 – 458, 2014. Cited on pages 7 and 21.

[5] Lino Guzzella and Antonio Sciarretta. *Vehicle Propulsion Systems: Introduction to Modeling and Optimization*. Springer, third edition, 2013. Cited on page 2.

[6] T. Huria, M. Ceraolo, J. Gazzarri, and R. Jackey. High fidelity electrical model with thermal dependence for characterization and simulation of high power lithium battery cells. In *Electric Vehicle Conference (IEVC), 2012 IEEE International*, March 2012. Cited on pages 3, 4, 5, and 31.

[7] R. Jackey, M. Saginaw, P. Sanghvi, and J. et al. Gazzarri. Battery model parameter estimation using a layered technique: An example using a lithium iron phosphate cell. In *SAE Technical Paper*, April 2013. Cited on pages 3, 4, 5, and 6.

[8] Long Lam and P. Bauer. Practical capacity fading model for li-ion battery cells in electric vehicles. *Power Electronics, IEEE Transactions on*, 28(12): 5910–5918, Dec 2013. ISSN 0885-8993. doi: 10.1109/TPEL.2012.2235083. Cited on pages 7, 14, and 15.

[9] Long Lam, P. Bauer, and E. Kelder. A practical circuit-based model for li-ion battery cells in electric vehicle applications. In *Telecommunications Energy Conference (INTELEC), 2011 IEEE 33rd International*, pages 1–9, Oct 2011. doi: 10.1109/INTLEC.2011.6099803. Cited on page 7.

[10] Jun Li, Edward Murphy, Jack Winnick, and Paul A Kohl. The effects of pulse charging on cycling characteristics of commercial lithium-ion batteries. *Journal of Power Sources*, 102(1–2):302 – 309, 2001. doi: http://dx.doi.org/10.1016/S0378-7753(01)00820-5. Cited on page 12.

[11] David Linden and Thomas Reddy. *Linden's Handbook of Batteries*. McGraw-Hill, fourth edition, 2011. Cited on pages 2, 4, and 8.